Subduction dynamics as revealed by trench migration

Serge Lallemand, Arnauld Heuret, C. Faccenna, F. Funiciello

Subduction dynamics as revealed by trench migration

Serge Lallemand,[1] Arnauld Heuret,[1] Claudio Faccenna,[2] and Francesca Funiciello[2]

Received 25 September 2007; revised 5 March 2008; accepted 28 April 2008; published 28 June 2008.

[1] New estimates of trench migration rates allow us to address the dynamics of trench migration and back-arc strain. We show that trench migration is primarily controlled by the subducting plate velocity V_{sub}, which largely depends on its age at the trench. Using the hot and weak arc to back-arc region as a strain sensor, we define neutral arcs characterized by the absence of significant strain, meaning places where the forces (slab pull, bending, and anchoring) almost balance along the interface between the plates. We show that neutral subduction zones satisfy the kinematic relation between trench and subducting plate absolute motions: $V_t = 0.5V_{sub} - 2.3$ (in cm a^{-1}) in the HS3 reference frame. Deformation occurs when the velocity combination deviates from kinematic equilibrium. Balancing the torque components of the forces acting at the trench indicates that stiff (old) subducting plates facilitate trench advance by resisting bending. **Citation:** Lallemand, S., A. Heuret, C. Faccenna, and F. Funiciello (2008), Subduction dynamics as revealed by trench migration, *Tectonics*, *27*, TC3014, doi:10.1029/2007TC002212.

1. Introduction

[2] A trench is the geographic location of a subduction plate boundary at a given time. This location may change over time as a result of global plate tectonics. *Carlson and Melia* [1984] stated that "back-arc tectonics is controlled principally by the difference in absolute motion between the overriding plate and the migration of the hinge of the downgoing plate." In this study, we test the hypothesis that trench migration is dependent on lower plate parameters in light of updated kinematic data. Since volcanic arcs or back arcs are generally hot and weak [e.g., *Currie and Hyndman*, 2006], we use this area as a sensor, represented by a spring in Figure 1, to determine the stress transmitted from one plate to the other. The lack of strain is supposed to indicate limited deviatoric stress, i.e., low stress transmission from one plate to the other through the interface between them. If no significant deformation occurs in the arc-back-arc region (normal component of deformation rate $v_d \approx 0$, neutral regime), then the subduction rate (v_s) equals the convergence rate between the major plates (v_c), and the velocity of the trench (V_t) equals the velocity of the upper plate (V_{up}). We use the respective plate motions to explore the kinematic conditions required for the absence of upper plate strain. Trench migration in such neutral subduction zones provides useful information about the balance of forces between the subducting plate and the mantle without significant interaction with the overriding plate. In contrast, if deformation occurs ($v_d \neq 0$), the subduction rate will depend on both the convergence velocity between the major plates (v_c) and the deformation velocity (v_d). We can therefore explore the kinematic criteria that characterize subduction zones when the trench moves spontaneously, i.e., neutral subduction zones, and those experiencing active shortening or spreading and ultimately infer the dynamic equilibrium of forces along the interface between the plates.

2. Data

[3] We use the global database already published in work by *Heuret and Lallemand* [2005] and *Lallemand et al.* [2005], which consists of transects every 2° of latitude/longitude (≈200 km) along subduction zones. From this database, we have excluded the transects where continental crust, ridges, or plateaus subduct and those with slabs narrower than 500 km. This exclusion focused our study on 166 transects (see Table 1). We use the normal component of velocity. Upper plate strain is determined from focal mechanisms of earthquakes occurring at a depth of less than 40 km from the surface of the upper plate, far from the subduction interface. We have simplified the seven strain classes described by *Heuret and Lallemand* [2005] into three: E3 and E2 become extensional (rifting or spreading); E1, 0, and C1 become neutral (no significant deformation or strike slip); and C2 and C3 become compressional (shortening).

[4] We distinguish between v_s, V_{up}, V_t, and V_{sub} to describe the velocities of subduction, of the upper plate, the trench, and the subducting plate, respectively. We estimate V_t by subtracting the deformation velocity v_d as estimated by geodetic measurements from V_{up}, neglecting erosion and accretion at the toe of the margin's wedge. Velocity is estimated using three different reference frames: NNR [*DeMets et al.*, 1994; *Gripp and Gordon*, 2002], SB04 [*Steinberger et al.*, 2004; *Becker*, 2006], and HS3 [*Gripp and Gordon*, 2002]. These three models span the whole range of net rotation of the lithosphere with respect to the mantle important to the kinematic relationships [e.g., *Doglioni et al.*, 2007]. Finally, because our study is mainly focused on Pacific subduction zones, we prefer a reference frame that includes Pacific hot spot analysis, such as the HS3.

[1]UMR 5573, CNRS, Laboratoire Géosciences Montpellier, Montpellier II Université, Montpellier, France.
[2]Dipartimento di Scienze Geologiche, Università degli Studi Roma TRE, Roma, Italy.

0278-7407/08/2007TC002212

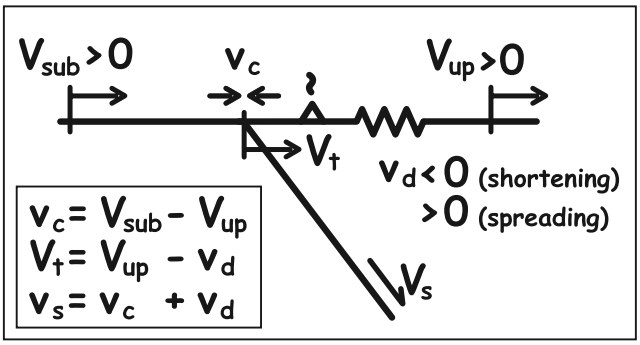

Figure 1. Definition of velocities in a schematic subduction zone. A weak arc is compared with a spring that deforms at a rate v_d (positive for spreading). And v_c is the relative plate convergence rate. Subduction rate v_s is the sum of convergence rate v_c and deformation rate v_d. V_{up}, V_t, and V_{sub} are the absolute upper plate, trench, and subducting plate motions counted positive landward. Upper case velocities are absolute, and lower case velocities are relative.

2.1. Trench Migration

[5] Quantitative estimates of trench motion are done in a given reference frame. For a long time, scientists considered that trenches should migrate spontaneously seaward with respect to a passive underlying mantle, so-called trench rollback, as a consequence of the downward pull exerted by the excess mass of slabs in the mantle [*Molnar and Atwater*, 1978; *Dewey*, 1980; *Garfunkel et al.*, 1986]. Back arc spreading was thus associated with trench rollback [e.g., *Molnar and Atwater*, 1978]. However, some authors noticed early on that trenches might advance toward the arc [e.g., *Carlson and Melia*, 1984; *Jarrard*, 1986; *Otsuki*, 1989]. Recently, updated estimates of trenches' motion have become available, based on a new global database of all oceanic subduction zones [*Heuret and Lallemand*, 2005]. Table 2 gives estimates for three different reference frames. Depending on the reference frame, the mean net rotation of the lithosphere with respect to the mantle varies from 0 (NNR) to 3.8 cm a^{-1} (HS3), resulting in a global tendency for slabs to retreat (rollback) at mean rates varying from 1.1 ± 3.0 (NNR) to 0.6 ± 3.0 cm a^{-1} (HS3). The maximum rate of trench rollback is in the northern Tonga region (12.5 (SB04) to 14.5 cm a^{-1} (HS3)). The main effect of net rotation is found in the ratio between advancing and retreating trenches, even if retreating rates are faster on average than advancing ones. Thirty percent of trenches in SB04 are prograding toward arcs. This number becomes 39% using NNR and 53% using HS3 reference frame. In HS3 reference frame, 50% of modern back-arc basins open above advancing trenches, and more generally, back-arc deformation scales with the absolute motion of the upper plate [*Heuret and Lallemand*, 2005]. In addition, trench (hinge) velocity scales with (subducting) plate velocity in a retreating mode for low plate velocities and an advancing mode for fast ones (Figure 2) [*Heuret*, 2005; *Faccenna et al.*, 2007]. This correlation, although less pronounced, also holds for NNR and SB04 reference models [*Funiciello et al.*, 2008].

[6] This global kinematic relationship has been poorly investigated, possibly because the dynamics of advancing trenches have never been accurately reproduced. Recently, *Bellahsen et al.* [2005], *Schellart* [2005], *Funiciello et al.* [2008], and *Di Giuseppe et al.* [2008] observed that both advancing and retreating subduction can be obtained in the laboratory, depending on physical parameters such as plate thickness, stiffness, width, velocity, mantle viscosity, and tank height. In addition, the experimental scaling relationships between plate and trench velocity have been used to predict the global trench and plate velocity using the radius of curvature and the age of the plate at the trench [*Faccenna et al.*, 2007].

[7] To summarize, trench migrations occur in both directions (arcward or seaward) for modern subduction zones. In most cases, trench velocities correlate with subducting plate velocities: retreating and advancing modes are preferentially observed for slow and fast subducting plates, respectively (Figure 2).

2.2. Relationship Between Upper and Subducting Plate Velocities and Slab Age at Trench

[8] In this study, on the basis of modern subduction zone observations, we consider the subducting plate velocity results from a 3-D dynamic equilibrium between negative buoyancy of the slab and the resisting forces both in the lithosphere (bending and shear) and in the mantle [*Forsyth and Uyeda*, 1975]. We also consider that the trench migration V_t mainly depends on V_{sub}, as shown in Figure 2. Conversely, the main overriding plate velocity V_{up} also results from a 3-D balance of forces, which can be far-field with respect to the subduction zone. For example, the northwestern motion of the Philippine Sea plate with respect to Eurasia is largely due to the pull exerted by the Ryukyu slab and is not influenced as much by its coupling with the Pacific plate at the Izu-Bonin-Mariana trench, by lateral density, or by topographic variations [*Pacanovsky et al.*, 1999]. On a plot of the motion of the main overriding plate V_{up} versus that of the subducting plate V_{sub} for modern oceanic subduction zones in the HS3 reference frame (Figure 3), *Heuret* [2005] observed that these parameters are correlated.

[9] First of all, 98% of normal components of convergence velocities v_c between major plates are between 0 and 10 cm a^{-1}. Second, all transects characterized by subducting oceanic plates older than 70 Ma are associated with retreating overriding plates. These two first-order observations led *Heuret* [2005] to propose the following empirical law: $v_c = V_{sub} - V_{up} = 5 \pm 5$ cm a^{-1}. This can be reached either by an old and fast lower plate subducting beneath a retreating overriding plate (e.g., Izu-Bonin-Mariana) or by young and slow plate subducting beneath an advancing upper plate (e.g., Andes, see insert of Figure 3). Changing the reference frame distorts the distribution of velocities slightly and thus the regression slope but does not alter the

Table 1. Data Set for 166 Transects Across Oceanic Subduction Zones[a]

Reference Frame Transects	HS3			SB04			NNR			Slab Age at Trench	Upper Plate Strain	Main Upper Plate
	V_{subn}	V_{upn}	V_{tn}	V_{subn}	V_{upn}	V_{tn}	V_{subn}	V_{upn}	V_{tn}			
ANDA6	−22.4	2.4	−24.4	7	27	5	24	44	22	85.5	1	Sunda
ANDA5	−11.7	1	−23.5	19	31	7	34	47	22	82	1	Sunda
ANDA4	−7. 2	2.1	−15.3	23	33	15	38	47	29	77.8	1	Sunda
ANDA3	12.6	8.5	−1.6	42	38	28	53	49	39	73.7	1	Sunda
ANDA2	19	10.3	−3.9	48	39	32	55	47	40	69.2	0	Sunda
ANDA1	27.4	12.6	7	53	38	33	60	45	39	61.1	0	Sunda
SUM6	57	18.4	18.4	70	31	31	64	25	25	51.8	0	Sunda
SUM5	37.9	12.7	12.7	61	36	36	64	39	39	46.2	0	Sunda
SUM4	46.3	14.5	14.5	67	35	35	67	35	35	47.1	0	Sunda
SUM3	46.4	12.7	12.7	66	33	33	67	34	34	60	0	Sunda
SUM2	47.2	12.3	12.3	67	32	32	68	33	33	69	0	Sunda
SUM1	60.9	14.6	14.6	74	27	27	70	23	23	72	0	Sunda
JAVA7	63.9	14.7	14.7	75	26	26	70	21	21	75	0	Sunda
JAVA6	69.7	14.6	14.6	77	22	22	70	15	15	78	0	Sunda
JAVA5	74.7	15.7	15.7	75	16	16	64	5	5	80	0	Sunda
JAVA4	75.6	14.7	14.7	76	15	15	65	4	4	81	0	Sunda
JAVA3	76.8	14.8	14.8	76	13	13	63	1	1	82	0	Sunda
JAVA2	77.4	13.6	13.6	77	13	13	66	2	2	83	0	Sunda
JAVA1	78.8	13	13	72	6	6	58	−8	−8	84	0	Sunda
LUZ4	11.3	−54.1	−33.5	37	−31	−8	42	−26	−3	22	−1	Phil. Sea
LUZ3	6.6	−88	−67.7	38	−57	−36	53	−43	−21	18	−1	Phil. Sea
LUZ2	8.6	−80.3	−81.3	40	−49	−50	52	−37	−38	27	−1	Phil. Sea
LUZ1	1.6	−95.8	−94	33	−64	−66	50	−47	−49	32	−1	Phil. Sea
BAT2	12	−59.8	−59.8	41	−31	−31	49	−23	−23	35	−1	Phil. Sea
PHIL7	72.3	−7.4	56.8	49	−31	33	43	−36	28	50	−1	Sunda
PHIL6	70	−8.3	51.7	47	−32	29	42	−38	23	50	−1	Sunda
PHIL5	91.8	−5.8	62.3	63	−35	33	51	−47	22	50	−1	Sunda
PHIL4	74.4	−8.9	44.1	48	−36	17	41	−43	10	50	−1	Sunda
PHIL3	64.8	−10	19.1	40	−35	−6	34	−40	−11	50	−1	Sunda
PHIL2	63	−10.9	4.2	37	−36	−21	31	−42	−27	45	−1	Sunda
RYUS	63.9	13.8	−30.3	49	−2	−46	32	−19	−63	35	1	Eurasia
RYUN1	77	17.5	−9	52	−6	−34	33	−24	−53	38	1	Eurasia
RYUN2	75.5	20.5	−11.8	48	−7	−39	30	−25	−58	48	1	Eurasia
RYUN3	74.4	21.1	−6.6	44	−9	−37	27	−26	−54	50	1	Eurasia
RYUN4	69.8	20.5	−9	38	−10	−41	22	−26	−57	50	1	Eurasia
NAN3	56.3	9.4	9.4	33	−13	−13	16	−30	−30	17	0	Amur
NAN2	50.8	9	9	30	−11	−11	14	−28	−28	17	0	Amur
NAN1	45.3	8.2	8.2	26	−10	−10	11	−26	−26	21	0	Amur
SMAR5	45.7	37.5	37.5	33	25	25	19	11	11	155	1	Phil. Sea
SMAR4	61.6	46.6	46.6	45	30	30	29	14	14	155	1	Phil. Sea
SMAR3	85.8	62.2	30.7	62	38	7	45	21	−10	156	1	Phil. Sea
SMAR2	109.9	79.7	43.9	79	49	13	62	32	−4	156.3	1	Phil. Sea
SMAR1	117.6	86	47.9	85	53	15	70	38	0	153.2	1	Phil. Sea
NMAR4	108.6	78	46.1	78	48	19	68	37	8	149.6	1	Phil. Sea
NMAR3	97.8	68.4	56.6	70	41	29	63	34	22	147.5	1	Phil. Sea
NMAR2	60.8	40.8	33.6	44	24	17	44	24	16	146.6	1	Phil. Sea
NMAR1	44.4	26.5	26.6	32	14	14	34	16	16	145.3	1	Phil. Sea
IZU4	109.2	60.2	60.2	78	29	29	68	19	19	148	1	Phil. Sea
IZU3	88	43.1	43.1	63	18	18	59	14	14	141	1	Phil. Sea
IZU2	95	43.8	43.8	68	16	16	62	11	11	135	1	Phil. Sea
IZU1	97.4	42.4	42.4	69	14	14	63	8	8	129	1	Phil. Sea
JAP4	113.7	11.9	21.2	82	−20	−10	68	−34	−24	127	−1	Amur
JAP3	111.6	11.9	20	80	−20	−11	67	−33	−24	132	−1	Amur
JAP2	105.9	10.7	20	75	−20	−12	67	−28	−20	131	−1	Amur
JAP1	109.8	11	19.6	78	−21	−12	67	−32	−23	128	−1	Amur
SKOUR5	100	23.3	23.3	72	−5	−5	57	−20	−20	128	−1	N-Amer.
SKOUR4	95.4	21.9	21.9	68	−5	−5	54	−19	−19	120	−1	N-Amer.
SKOUR3	99.3	22.3	22.3	71	−6	−6	57	−20	−20	118	−1	N-Amer.
SKOUR2	89.6	18.8	18.8	64	−7	−7	50	−21	−21	118	−1	N-Amer.
SKOUR1	98.2	20.7	20.7	70	−7	−7	57	−20	−20	118	−1	N-Amer.
NKOUR3	101.1	21.7	21.7	71	−8	−8	61	−18	−18	110	0	N-Amer.
NKOUR2	96.9	18.9	18.9	69	−9	−9	58	−20	−20	110	0	N-Amer.
NKOUR1	96	19.2	19.2	68	−9	−9	60	−17	−17	110	0	N-Amer.
KAM2	92.6	17.7	17.7	66	−9	−9	59	−16	−16	100	0	N-Amer.
KAM1	90.5	16.7	16.7	64	−10	−10	58	−16	−16	100	0	N-Amer.
W_ALE1	17.3	−4.6	−4.6	12	−10	−10	3	−19	−19	45	0	N-Amer.
W_ALE2	34.5	−1.6	−1.6	24	−12	−12	15	−21	−21	45	0	N-Amer.

Table 1. (continued)

Reference Frame Transects	HS3			SB04			NNR			Slab Age at Trench	Upper Plate Strain	Main Upper Plate
	V_{subn}	V_{upn}	V_{tn}	V_{subn}	V_{upn}	V_{tn}	V_{subn}	V_{upn}	V_{tn}			
C_ALE1	28.79	3.4	3.4	20	−12	−12	11	−21	−21	54	0	N-Amer.
C_ALE2	41.9	0.8	0.8	29	−14	−14	20	−22	−22	56	0	N-Amer.
C_ALE3	53.6	1.6	1.6	47	−15	−15	39	−22	−22	58	0	N-Amer.
C_ALE4	65.2	5	5	46	−14	−14	38	−23	−23	58	0	N-Amer.
C_ALE5	66	4.6	4.6	45	−15	−15	37	−23	−23	58	0	N-Amer.
C_ALE6	62.8	3.3	3.3	44	−15	−15	37	−23	−23	63	0	N-Amer.
E_ALE1	71.3	6	6	50	−15	−15	44	−21	−21	63	0	N-Amer.
E_ALE2	73	7.3	7.3	51	−15	−15	46	−19	−19	61	0	N-Amer.
E_ALE3	70.9	6	6	49	−15	−15	45	−20	−20	59	0	N-Amer.
E_ALE4	70	5.7	5.7	48	−16	−16	44	−20	−20	58	0	N-Amer.
E_ALE5	67.9	4.8	4.8	47	−16	−16	43	−20	−20	53	0	N-Amer.
W_ALA1	65.1	3.7	3.7	44	−17	−17	41	−20	−20	52	0	N-Amer.
W_ALA2	63.7	3.2	3.2	44	−16	−16	41	−20	−20	52	0	N-Amer.
W_ALA3	62.4	3	3	43	−17	−17	40	−19	−19	52	0	N-Amer.
W_ALA4	65	7	7	45	−13	−13	45	−13	−13	52	0	N-Amer.
W_ALA5	62.5	4.5	4.5	44	−14	−14	43	−15	−15	49	0	N-Amer.
E_ALA1	60.7	4.1	4.1	42	−15	−15	42	−14	−14	46	0	N-Amer.
E_ALA2	57.6	6.2	6.2	40	−12	−12	42	−10	−10	45	0	N-Amer.
E_ALA3	54.4	6.4	6.4	38	−10	−10	41	−7	−7	40	0	N-Amer.
E_ALA4	49.7	6.8	6.8	34	−9	−9	38	−5	−5	39	0	N-Amer.
E_ALA5	50.5	−1.5	−1.5	35	−17	−17	35	−17	−17	39	0	N-Amer.
CASC1	25	−21	−18.8	29	−17	−14	28	−18	−16	5	0	N-Amer.
CASC2	16.5	−22	−19.7	22	−17	−15	21	−18	−15	10	0	N-Amer.
CASC3	7.5	−23.8	−22.8	16	−16	−15	15	−16	−15	11	0	N-Amer.
CASC4	0.3	−24	−24	12	−13	−13	11	−13	−13	11	0	N-Amer.
CASC5	−2.7	−25.3	−23.9	9	−14	−12	9	−14	−12	10	0	N-Amer.
MEX1	4	−35.7	−35.7	18	−22	−22	29	−11	−11	8	0	N-Amer.
MEX2	17.8	−29.7	−29.7	25	−22	−22	37	−11	−11	8	0	N-Amer.
MEX3	26.4	−25.1	−25.1	31	−20	−20	43	−9	−9	15	0	N-Amer.
MEX4	32.5	−23.2	−23.2	36	−21	−21	49	−8	−8	15	0	N-Amer.
MEX5	37.8	−21.7	−21.7	41	−19	−19	53	−7	−7	15	0	N-Amer.
MEX6	43.9	−16.7	−16.7	44	−16	−16	56	−5	−5	15	0	N-Amer.
COST1	42.2	−21.4	−21.4	52	−12	−12	65	2	2	18	0	Carribean
COST2	49	−19.6	−19.6	57	−11	−11	72	3	3	22	0	Carribean
COST3	54.5	−18.5	−18.5	62	−11	−11	76	3	3	24	0	Carribean
COST4	55.3	−22.3	−22.3	67	−11	−11	82	4	4	28	0	Carribean
COST5	62	−21.6	−21.6	74	−9	−9	90	6	6	26	0	Carribean
COL1	14.9	−38.6	−27.4	39	−15	−3	44	−9	2	19	−1	S-Amer.
COL2	13.6	−35.9	−33	36	−13	−10	40	−10	−7	15	−1	S-Amer.
COL3	16.1	−38.2	−25.2	41	−13	0	46	−8	5	12	−1	S-Amer.
PER1	22.5	−46.6	−46.6	51	−18	−18	64	−5	−5	30	−1	S-Amer.
PER2	23.9	−47	−47	54	−17	−17	68	−3	−3	30	−1	S-Amer.
PER3	24.8	−45.9	−45.9	53	−17	−17	70	−1	−1	31	−1	S-Amer.
PER4	25.1	−45.1	−45.1	53	−17	−17	71	0	0	31	−1	S-Amer.
PER5	25.5	−43.8	−43.8	52	−17	−17	70	1	1	46	−1	S-Amer.
PER6	26	−42.6	−42.6	52	−16	−16	71	2	2	46	−1	S-Amer.
NCHI1	23.7	−34.4	−34.4	45	−13	−13	64	6	6	52	−1	S-Amer.
NCHI2	28.9	−43.6	−34.6	57	−15	−6	76	3	12	54	−1	S-Amer.
NCHI3	30.3	−47.9	−41.9	63	−15	−9	78	−1	5	55	−1	S-Amer.
NCHI4	29.5	−46.6	−41.8	62	−14	−9	74	−2	2	54	−1	S-Amer.
NCHI5	29.8	−46.9	−41	62	−14	−8	75	−2	4	53	−1	S-Amer.
NCHI6	29.1	−45.1	−39.4	61	−14	−8	71	−3	3	52	−1	S-Amer.
JUAN1	29.8	−44.6	−38.9	62	−13	−7	72	−2	4	49	−1	S-Amer.
JUAN3	31.8	−45.7	−38.8	64	−13	−7	76	−1	5	48	−1	S-Amer.
SCHI1	26.7	−38.9	−38.9	55	−10	−10	62	−3	−3	42	0	S-Amer.
SCHI2	25.1	−36.5	−36.5	53	−9	−9	58	−3	−3	39	0	S-Amer.
SCHI3	30.6	−42	−42	62	−11	−11	70	−2	−2	35	0	S-Amer.
SCHI4	32.5	−43	−43	64	−11	−11	75	−1	−1	33	0	S-Amer.
SCHI5	32.9	−43.3	−43.3	64	−12	−12	76	0	0	20	0	S-Amer.
TRI1	33.3	−42.7	−42.7	65	−11	−11	77	1	1	12	0	S-Amer.
TRI2	34.4	−41.7	−41.7	66	−10	−10	77	1	1	5	0	S-Amer.
TRI3	−19.4	−40.2	−40.2	12	−6	−6	22	5	5	10	0	S-Amer.
TRI4	−19.9	−40.8	−40.8	11	−10	−10	21	1	1	18	0	S-Amer.
PAT1	−21.7	−41	−41	9	−10	−10	24	4	4	18	0	S-Amer.
PAT2	−20.8	−39.6	−39.6	10	−9	−9	22	3	3	20	0	S-Amer.
PAT3	−20.3	−32.3	−32.3	3	−9	−9	20	8	8	20	0	S-Amer.
BARB1	40.8	28.1	28.1	17	5	5	8	−5	−5	117	0	Carribean

Table 1. (continued)

Reference Frame Transects	HS3			SB04			NNR			Slab Age at Trench	Upper Plate Strain	Main Upper Plate
	V_{subn}	V_{upn}	V_{tn}	V_{subn}	V_{upn}	V_{tn}	V_{subn}	V_{upn}	V_{tn}			
BARB2	41.7	29.8	29.8	18	6	6	3	−9	−9	110	0	Carribean
ANTI1	41.8	31	31	18	7	7	3	−8	−8	98	0	Carribean
ANTI2	37.2	27.6	27.6	16	6	6	−1	−11	−11	90	0	Carribean
ANTI3	26.4	20.5	20.5	12	6	6	−6	−11	−11	84	0	Carribean
PORTO1	14.7	11.7	6.6	7	4	−1	−8	−11	−16	92	0	Carribean
PORTO2	8.5	7.3	1.3	5	3	−2	−8	−10	−15	100	0	Carribean
PORTO3	8.5	7.3	1.3	5	4	−2	−7	−9	−14	110	0	Carribean
SAND1	17.8	15.7	−17.9	3	3	−36	12	12	−27	33	1	Scotia
SAND2	29	24.4	−49	5	1	−73	4	−1	−74	36	1	Scotia
SAND3	33	26.9	−39.4	6	0	−63	−2	−8	−71	40	1	Scotia
SAND4	26.6	20.8	-8.5	4	−2	−32	−9	−15	−44	40	1	Scotia
SAND5	17	13.2	1.9	1	−2	−14	−12	−16	−27	40	1	Scotia
SAND6	20.6	15.8	17	3	−2	−1	−11	−16	−15	40	0	Scotia
MAK2	30.7	−6	15.6							99	0	Eurasia
MAK3	35	−2	19							98	0	Eurasia
MAK4	37.1	-0.4	21							97	0	Eurasia
KER1	100.3	53.7	53.7	73	27	27	54	8	8	95	1	Australia
KER2	100.4	49	49	73	21	21	55	4	4	97	1	Australia
KER3	104.1	49.8	49.8	76	22	22	58	4	4	99	1	Australia
KER4	104.5	44.9	44.9	76	16	16	58	−2	−2	101	1	Australia
KER5	103.5	39.4	39.4	76	12	12	58	−6	−6	103	1	Australia
TONG2	111.9	47	8	81	16	−23	63	−2	−41	106	1	Australia
TONG3	112.6	40.4	−40.4	82	10	−67	64	−8	−85	107	1	Australia
TONG4	112.4	35.2	−69.7	82	4	−107	65	−12	−124	108	1	Australia
TONG5	109.6	35.2	−113.6	82	3	−104	66	−14	−121	108	1	Australia
SHEB2	17.6	−56.6	−101	33	−40	−85	41	−33	−78	45	1	Pacific
SHEB3	−3.2	−85.4	−96.1	19	−63	−74	32	−50	−61	48	1	Pacific
NHEB1	−2.5	−90.6	−105.1	22	−67	−81	34	−54	−69	60	1	Pacific
NHEB2	20.8	−67.4	−144.7	39	−50	−125	47	−41	−117	60	1	Pacific
BRET3	100.5	90.4	−19.5	76	64	−44	59	48	−61	31	1	n-Bism.
BRET2	92.7	94.4	17.5	74	72	−9	57	55	−26	31	1	n-Bism.
BRET1	86	38	22	78	29	13	67	18	2	31	1	n-Bism.

[a]All velocities are expressed in mm a^{-1}. V_{subn}, V_{upn}, and V_{tn} (simply called V_{sub}, V_{up}, and V_t in the text) are the normal components of the subducting plate, upper plate, and trench in the three reference frames NNR, SB04, and HS3. Age is given in Ma. Back-arc strain is 1 for extension, 0 for neutral, and −1 for compression as deduced from the study of focal mechanisms of earthquakes (see *Heuret and Lallemand* [2005] for further details). Phil. Sea, Philippine Sea; N-Amer., North America; S-Amer., South America; N-Bism., north Bismarck.

empirical law regarding v_c or the fact that old slabs are correlated with fast subducting plates.

2.3. Relationship Between the Combination of Upper and Subducting Plate Velocities and Upper Plate Strain

[10] Given the conclusions that V_{up} and V_{sub} are not distributed randomly but are combined, such as $V_{sub} \approx V_{up}$ + 5 cm a^{-1}, we can now examine their combination with respect to upper plate strain: extensional, neutral, or compressional. We have plotted the results for the 166 transects in the HS3 reference frame (Figure 4a) but also in the two other reference frames discussed in section 2.1 (NNR, SB04) (Figures 4b and 4c) for comparison.

[11] Let us first discuss the results in the HS3 reference frame. Obviously, the (V_{up} and V_{sub}) combinations of velocities are not randomly distributed with respect to the associated upper plate strain. We distinguish three elongated domains, all three of which possess positive slopes (Figures 4a and 4b):

[12] 1. The first is a domain of kinematic equilibrium where neither compressional nor extensional deformation is observed. The equation of the regression line for neutral transects (the neutral line) is

$$V_{up} = 0.5V_{sub} - 2.3$$

$$\text{or} \quad V_{sub} - 2V_{up} = 4.6 \ \left(\text{in cm a}^{-1}\right).$$

Along this line, the velocity of the trench (V_t) equals the velocity of the upper plate (V_{up}) because no deformation occurs: $v_d = 0$. We can thus write

$$V_t = 0.5V_{sub} - 2.3$$

only for those subduction zones with no upper plate deformation.

[13] 2. The second is a domain where active shortening is observed in the overriding plate. Transects in this domain satisfy the relation $V_{up} < 0.5V_{sub} - 2.3$. Compression within the overriding plate occurs not only for trenchward moving upper plates, but also for retreating main overriding plate, like in NE Japan.

Table 2. Characteristics of Trench Motions in Three Reference Frames

Reference Frame	NNR-NUVEL1A [*Gripp and Gordon*, 2002]	SB04 [*Steinberger et al.*, 2004]	HS3-NUVEL1A [*Gripp and Gordon*, 2002]
Selected hot spots	no hot spots	Indo-Atlantic hot spots	Pacific hot spots
Age of hot spots	-	80 Ma–present	5.8 Ma–present
Mean/maximum net rotation	0 by definition	1.4/1.8 cm a^{-1}	3.8/4.9 cm a^{-1}
Mean trench motion	1.1 ± 3.0 cm a^{-1} (rollback)	0.9 ± 3.0 cm a^{-1} (rollback)	0.6 ± 4.0 cm a^{-1} (rollback)
Maximum rate of trench rollback	12.7 cm a^{-1}	12.5 cm a^{-1}	14.5 cm a^{-1}
Maximum rate of trench advance	5.1 cm a^{-1}	6.9 cm a^{-1}	9.7 cm a^{-1}
Rollback/advance transects ratio	1.56	2.33	0.89

[14] 3. The third is a domain where active extension is observed in the overriding plate. Transects in this domain satisfy the relation $V_{up} > 0.5V_{sub} - 2.3$. We observe a single exception, i.e., the four transects across the New Hebrides trench, discussed in section 3.

[15] Figure 5 illustrates three specific combinations of velocities along the neutral line where $v_d = 0$, and thus $V_t = V_{up}$. We first consider a fixed subducting plate: the upper plate needs to advance at a rate of 2.5 cm a^{-1} to balance trench retreat. This case would correspond to the Cascades (see A on Figure 4a). In the second case, the upper plate and the trench are fixed, and the neutral regime is reached when the subducting plate moved trenchward at a rate of 5 cm a^{-1}. This case would correspond to the eastern Aleutians (see B on Figure 4a). The last case is a subducting plate moving trenchward at a rate of 10 cm a^{-1} and an upper plate retreating at 2.5 cm a^{-1}. This combination implies that the trench advances at the same rate as the upper plate retreat, i.e., 2.5 cm a^{-1}. This last case is similar to the northern Kurils (see C on Figure 4a). We thus see that the

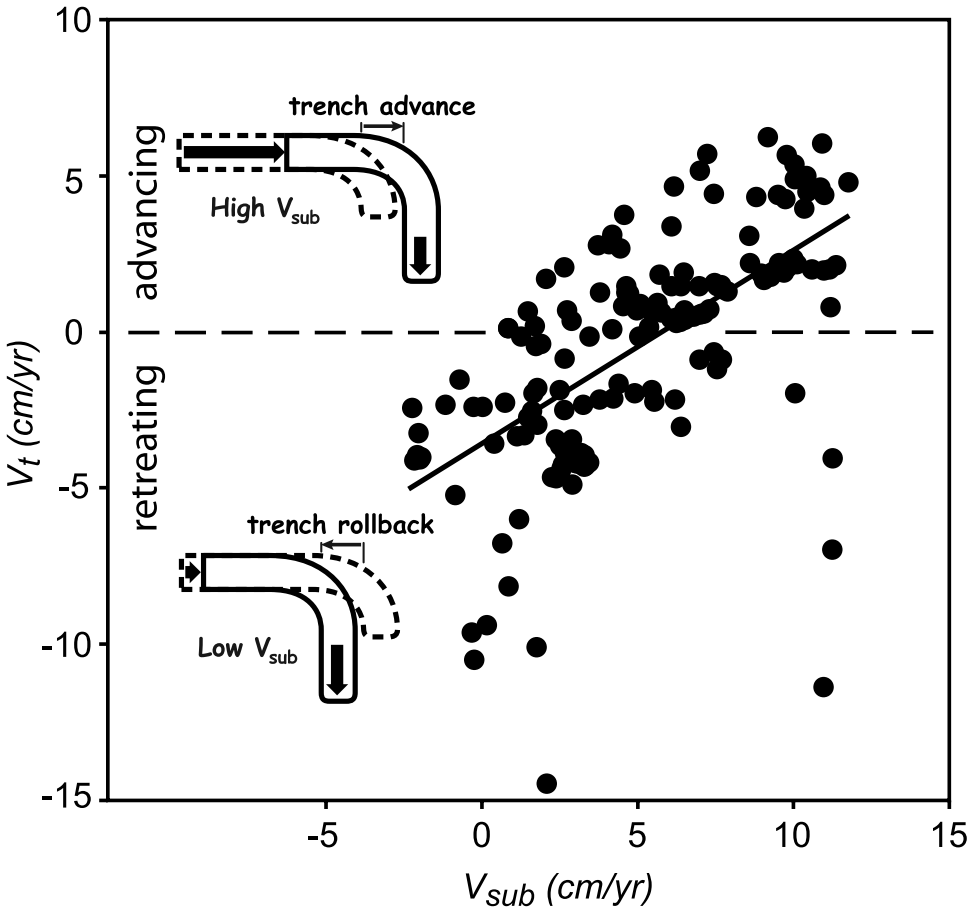

Figure 2. Correlation between the normal components of trench and subducting plate velocities in the HS3 reference frame for the 166 selected transects (see selection criteria in the main text). Fast subducting plates promote trench advance, whereas slow ones favor trench retreat. Regression line equation is $V_t = 0.62\ V_{sub} - 3.7$ in cm a^{-1} (quality factor $R^2 = 0.37$).

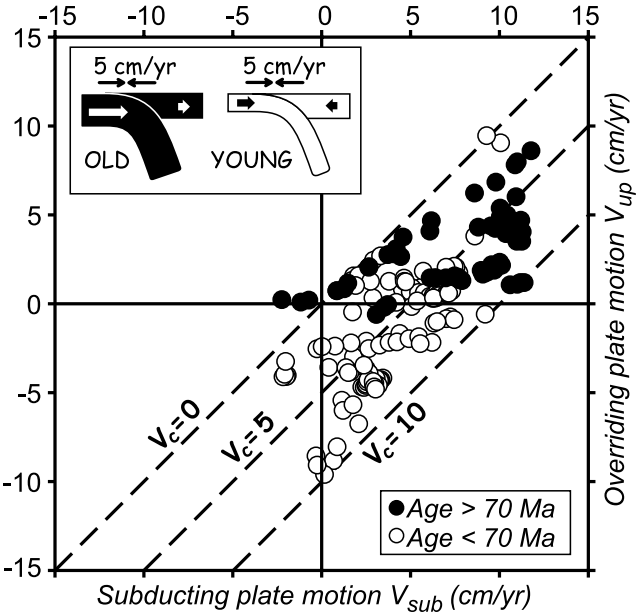

Figure 3. Overriding plate absolute motion V_{up} versus subducting plate absolute motion V_{sub} for the 166 selected transects. White dots are transects where slab age at trench is younger than 70 Ma, whereas black dots are for those older than 70 Ma. The diagram and the sketch inside the diagram are adapted from work by *Heuret* [2005].

neutral regime can be obtained with various combinations of plate and trench motions.

[16] In Figure 6 with a few modern examples, we illustrate the evolution of upper plate deformation (v_d) by varying the velocity of one of the converging plates while keeping the other one constant, i.e., an upper plate retreating at V_{up} = 1 cm a^{-1} (Figures 4a and 6a) and a subducting plate moving at a rate V_{sub} = 2 cm a^{-1} (Figures 4a and 6b). Large variations of V_{sub} (from 11 to 2 cm a^{-1} for V_{up} = 1 cm a^{-1}) produce shortening (e.g., NE Japan) or spreading (e.g., Sandwich) in the upper plate, and small variations of V_{up} (from −4 to 1 cm a^{-1} for V_{sub} = 2 cm a^{-1}) produce the same effect, i.e., shortening (e.g., Columbia) or spreading (e.g., Sandwich).

[17] Returning to the dependency of the results on the reference frame, we observe in Figures 4c (NNR) and 4d (SB04) that both V_{up} and V_{sub} show lower variations in HS3 as a result of little or no net rotation. Strangely, the slope V_{up}/V_{sub} as well as the quality of the regression on neutral transects, though less than for HS3 (V_{up}/V_{sub} = 0.46, and R^2 = 0.37), is better for NNR (V_{up}/V_{sub} = 0.32, and R^2 = 0.23) than for SB04 (V_{up}/V_{sub} = 0.24, and R^2 = 0.11). We still observe that compression is observed in the upper plate only for combinations of plate velocities below the neutral line (V_{up} < 0.3 V_{sub} − 1.9 for NNR and V_{up} < 0.2 V_{sub} − 1.4 for SB04). The New Hebrides are still located in the compressional domain for NNR. Some other extensional transects, like Ryukyu and Tonga, overlap with the neutral domain.

3. Discussion

[18] On the basis of this study, we observe that strain in the upper plate is predominantly controlled by its absolute motion [*Heuret and Lallemand*, 2005; *Heuret et al.*, 2007]. Indeed, the slope V_{up}/V_{sub} of the neutral line is 0.5, meaning that V_{up} is twice as influential on the tectonic regime of the upper plate as is V_{sub}. V_{up} thus dominates the control of back-arc stress but is not enough, as illustrated by NE Japan, which shows (in HS3) that a retreating upper plate can be counterbalanced by a fast subducting plate to produce back arc shortening. In other words, the kinematic conditions required to balance the arcward and oceanward forces applied along the interface between the plates with respect to the upper plate are satisfied when $V_{up} = 0.5V_{sub} - 2.3$, whenever the main upper plate (or the trench, because $V_t = V_{up}$ when $v_d = 0$) retreats or advances. Stress transmission and upper plate deformation occur when velocities deviate from this equilibrium.

[19] The New Hebrides transects do not satisfy the general rule in any of the chosen reference frames, in the sense that the combination of velocities V_{up}/V_{sub} predict a compressional regime and not an extensional one. This is undoubtedly due to the unique plate configuration in this complex area [see *Pelletier et al.*, 1998]; we have chosen the Pacific plate as the main upper plate, but the system is 3-D with several active spreading centers sandwiched between the Pacific plate to the north and the Australian plate to the west and southeast. This back-arc area is known for its multiridge activity caused by active upper mantle convection [*Lagabrielle et al.*, 1997]. We thus consider that mantle flow may disturb plate interactions.

[20] The Tonga subduction zone also warrants some discussion. The transects across this subduction zone fall into the extensional domain when using HS3 (Figure 4b) because the overriding Australian plate is retreating enough

Figure 4. Same diagrams as in Figure 3: V_{up} versus V_{sub}, but divided into three groups depending on the tectonic regime within the upper plate (see Table 1). (a) Velocities in HS3 reference frame. The regression line V_{up} = 0.5 V_{sub} − 2.3 in cm a^{-1} (or V_{sub} − 2 V_{up} = 4.6) is valid only for the neutral subduction zone transects (white dots). Quality factor R^2 = 0.37. Along the neutral line, the trench velocity V_t equals the upper plate velocity V_{up} because v_d = 0. All transects characterized by active compression are located below this line, and all transects characterized by active extension are located above the line. (b) Luz, Luzon; Col, Columbia; C-Am, Central America; Phil, Philippines; Kur, Kurils; Kam, Kamtchatka; Ker, Kermadec; Izu, Izu-Bonin; Ryu, Ryukyu; Mar, Mariana; Ant, Antilles; Sand, Sandwich; Sum, Sumatra; Nan, Nankai; Ale, Aleutians; Casc, Cascades; Pat, Patagonia; Ala, Alaska; Anda, Andaman; Mak, Makran; N-Heb, New Hebrides; N-Brit, New Britain. (c) The same diagram in NNR reference frame. The regression line equation is $V_{up} = 0.32V_{sub} - 1.9$. Quality factor R^2 = 0.23. (d) The same diagram in SB04 reference frame. The regression line equation is $V_{up} = 0.24V_{sub} - 1.4$. Quality factor R^2 = 0.23.

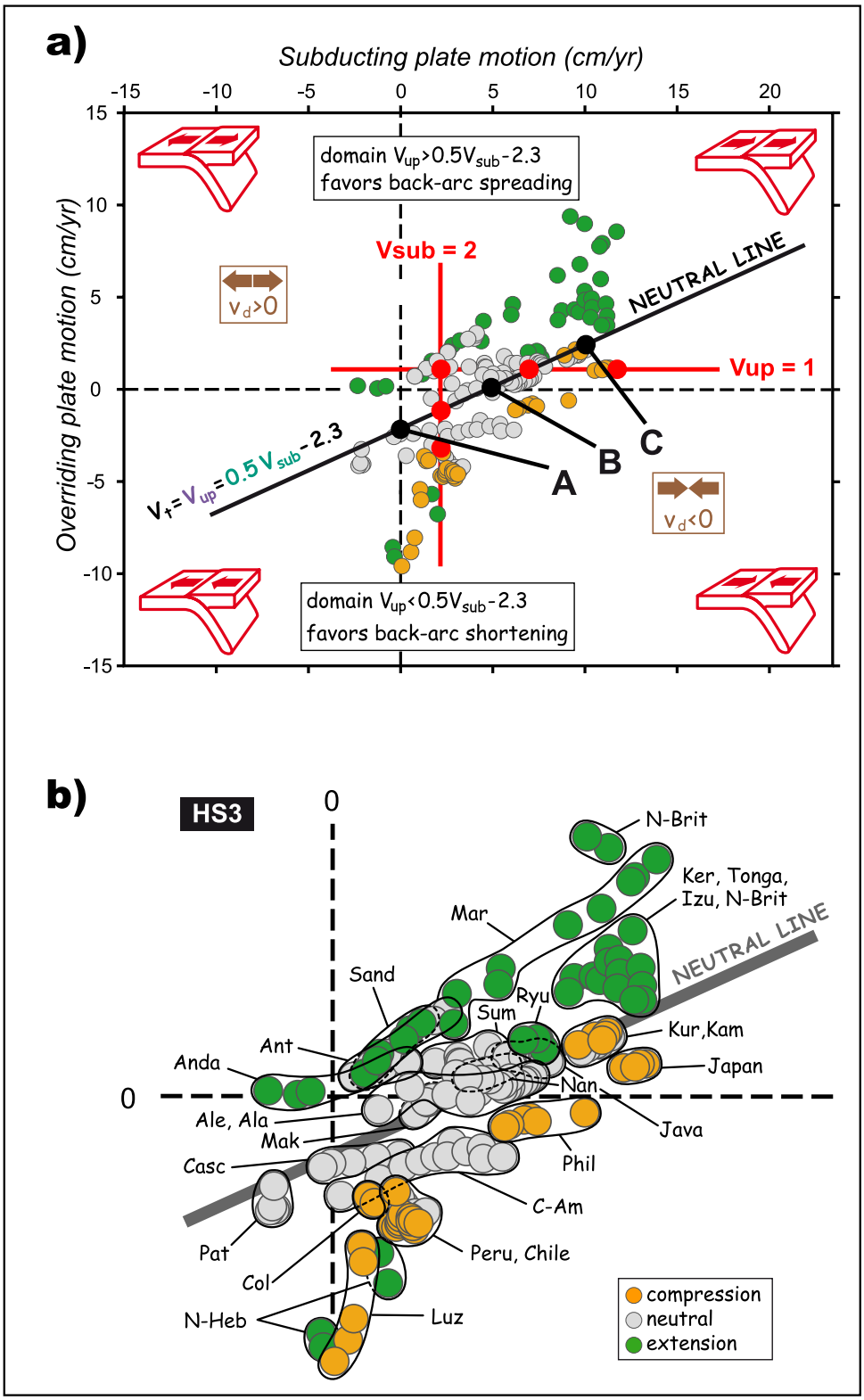
a)
Subducting plate motion (cm/yr)
Overriding plate motion (cm/yr)
domain V_{up}>0.5V_{sub}-2.3
favors back-arc spreading
Vsub = 2
NEUTRAL LINE
Vup = 1
v_d>0
V_r=V_{up}=0.5 V_{sub}-2.3
A
B
C
v_d<0
domain V_{up}<0.5V_{sub}-2.3
favors back-arc shortening
b)
HS3
N-Brit
Ker, Tonga,
Izu, N-Brit
Mar
NEUTRAL LINE
Sand
Ryu
Sum
Kur,Kam
Ant
Anda
Japan
Nan
Ale, Ala
Java
Mak
Casc
Phil
C-Am
Pat
Peru, Chile
Col
N-Heb
Luz
compression
neutral
extension

Figure 4

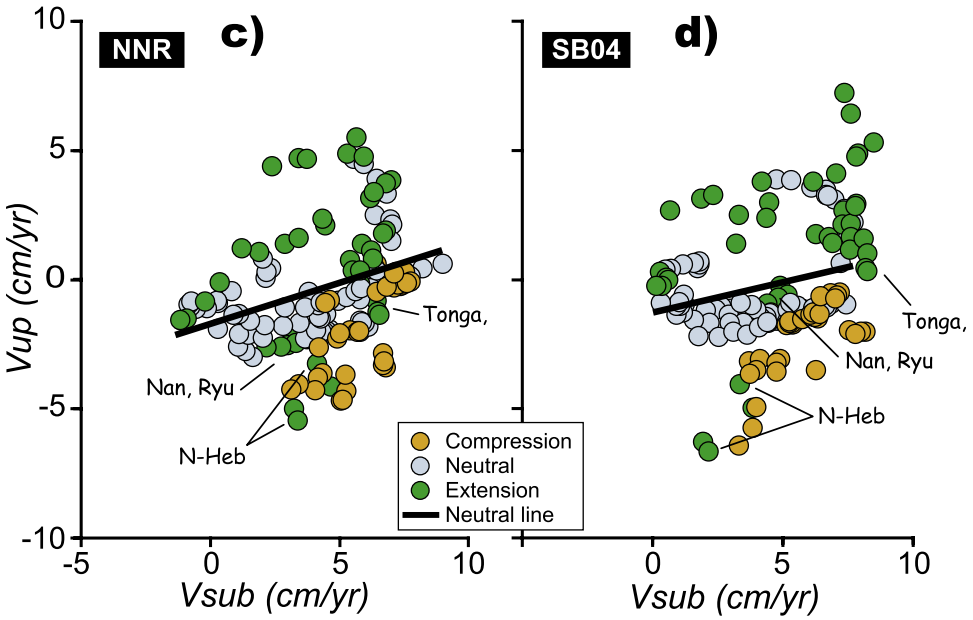

Figure 4. (continued)

to compensate the fast-moving Pacific plate. This is not true in the NNR or SB04 reference frames (see Figures 4c and 4d). As discussed by *Heuret and Lallemand* [2005], we consider this region (that includes the New Hebrides and Tonga arcs) to be subject to strong mantle flows, probably rising from active mantle convection beneath the North Fiji Basin [*Lagabrielle et al.*, 1997]. It is therefore not surprising that the transects here often deviate from general subduction rules.

3.1. Spontaneous Trench Motion

[21] The most informative result of this paper concerns the neutral domain where trench motion V_t equals upper plate motion V_{up}, which is approximately equivalent either to the absence of upper plate motion or to a trench motion that is not affected by the upper plate, at least in terms of stress transmission. In the case of the neutral regime ($v_d = 0$), trench motion depends only on the balance of forces between the subducting plate and the surrounding mantle. In Figure 5, we illustrate that spontaneous trench motion may vary with rollback, fixity, and advance by changing V_{sub}. Spontaneous trench motion is thus not only restricted to trench rollback, as suggested by *Chase* [1978] or *Hamilton* [2003]. This result is still valid in the NNR and SB04 reference frames, for which the Sunda trench (from Sumatra to Java) is advancing. *Funiciello et al.* [2004], *Bellahsen et al.* [2005], and *Di Giuseppe et al.* [2008] reached similar conclusions experimentally.

3.2. Interplate Coupling and Stress Transmission

[22] Another result of this study involves the source of interplate coupling and stress transmission from one plate to

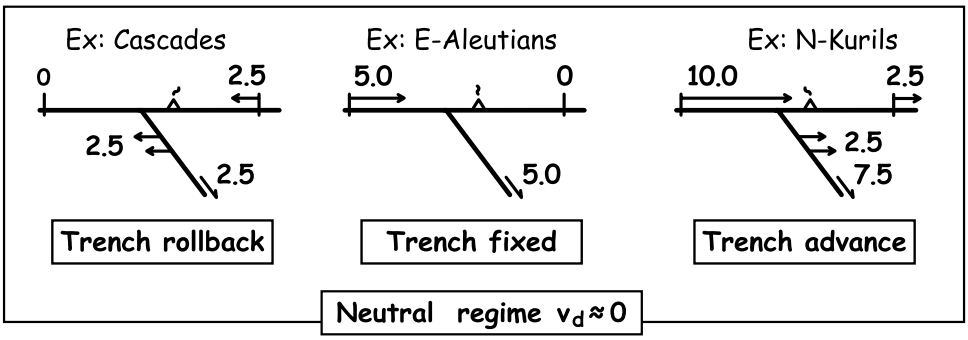

Figure 5. Three specific examples taken along the neutral line where the deformation rate v_d = 0, i.e., trench velocity V_t equals upper plate velocity V_{up}. See location of transects on the neutral line in Figure 4a. (left) Cascades with a fixed subducting plate producing trench rollback at a rate of 2.5 cm a^{-1}. (middle) Eastern Aleutians, upper plate (and thus trench) are fixed for a subducting plate moving at 5 cm a^{-1}. (right) Northern Kurils with a fast subducting plate (10 cm a^{-1}) inducing trench advance at a rate of 2.5 cm a^{-1}.

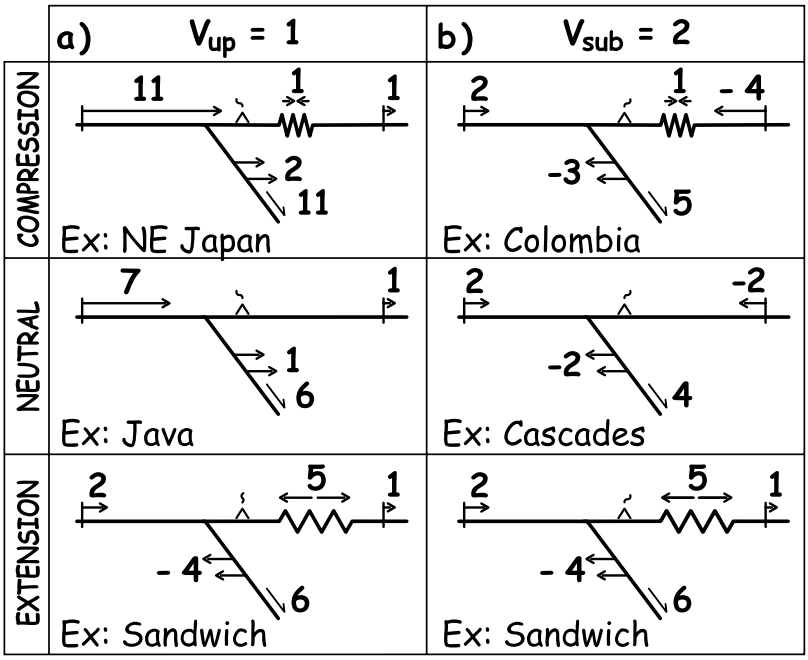

Figure 6. (a) Three specific examples for a constant upper plate retreat of 1 cm a^{-1}. Horizontal arrows indicate trench and slab motion. See Figure 1 for the definition of velocities and location of transects in Figure 4a. A dynamic equilibrium (neutral regime) is reached in Java. From the equation of kinematic equilibrium, we see that compression occurs when V_{sub} increases (NE Japan), and extension occurs when V_{sub} decreases (Sandwich). In the case of NE Japan, Pacific plate motion reaches 11 cm a^{-1}. Back arc shortening occurs at a rate of about 1 cm a^{-1}, so that the trench advances at 2 cm a^{-1}, and the subduction rate is 11+1 − 1 = 11 cm a^{-1}. (b) Three specific examples for a constant subducting plate trenchward advance of 2 cm a^{-1} (see location of transects in Figure 4a). In this case, dynamic equilibrium is reached when both plates advance trenchward at a rate of 2 cm a^{-1} (Cascades), compression occurs when V_{up} increases (trenchward motion, Colombia), and extension occurs when V_{up} decreases (arcward motion, Sandwich).

the other. We show here that compressional stress does not simply increase with increasing convergence velocity v_c but is also favored for moderate v_c when $V_{sub} < 0.5\ V_{up} - 2.3$. This is even more true for extensional stress, which can even be reached when v_c is large (e.g., v_c = 8 cm a^{-1} in Tonga), since $V_{sub} > 0.5\ V_{up} - 2.3$ remains true.

3.3. Forces Balance

[23] A long list of authors so far addressed the dynamical aspects of subduction/convection system from kinematic data [e.g., *Forsyth and Uyeda*, 1975; *McKenzie*, 1977; *Davies*, 1980; *Carlson*, 1995; *Conrad and Hager*, 1999; *Conrad and Lithgow-Bertelloni*, 2002; *Becker et al.*, 1999; *Buffett and Rowley*, 2006; *Faccenna et al.*, 2007; *Di Giuseppe et al.*, 2008], but the quantification of the different contributions in the subduction system remains elusive and dependent upon assumptions and somehow arbitrary scaling parameters.

[24] The analysis presented here, although not pretending to give exact quantification of the forces at work, first uses the mode of trench migration as a proxy for the competition between the different contributions. The slab/mantle system is here considered to result from the competition between arcward and oceanward forces acting on a slab, or more specifically, the folding and unfolding torques acting at the pivot made by the slab hinge. To better understand the role of the main forces, we will assume a constant radius of curvature R_c, slab length L, and dip α. We neglect the interaction of the slab with both the 660 km discontinuity and the lower mantle, which are extremely difficult to model because slab imagery at this depth is often unclear and difficult to interpret. We consider the change in slab dip to be negligible, so that trench motion equals horizontal slab migration.

[25] The correlation between the age of the subducting plate A and its absolute motion V_{sub} indicates that slab pull is the main force driving the motion of the subducting plate. Resisting forces are partitioned between mantle and lithosphere [*Conrad and Hager*, 1999]. We neglect friction and suction at the top of the slab since they are at least 1 order of magnitude smaller [*Turcotte and Schubert*, 1982; *Conrad and Hager*, 1999]. We assume that the upper mantle behaves passively as it is excited by slab subduction and migration. The asthenospheric mantle viscously resists to facewise translation of the slab, i.e., form drag. Finally, we distinguish three forces and related torques (see Figure 7).

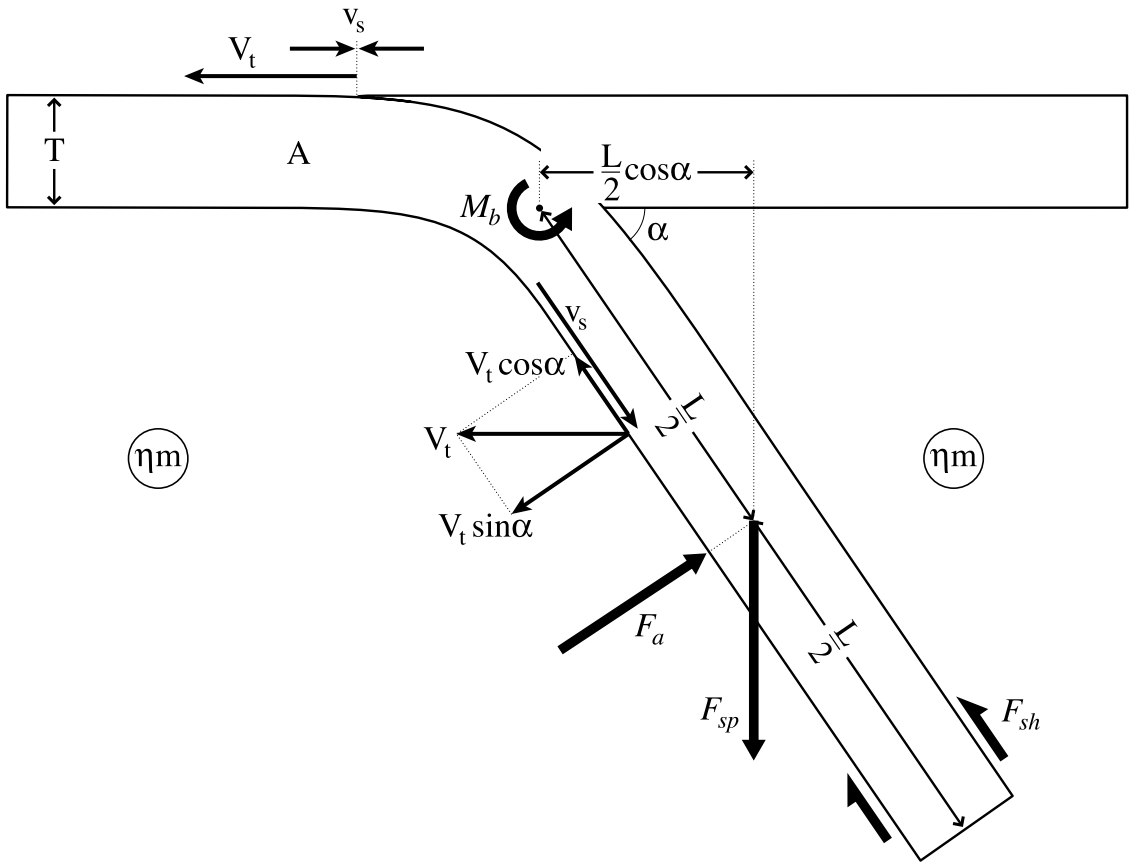

Figure 7. Sketch showing the velocities, forces, torques, and other parameters used in the notations.

[26] 1. The slab pull force F_{sp} represents the main driving force in the system [e.g., *Forsyth and Uyeda*, 1975; *McKenzie*, 1977; *Davies*, 1980; *Carlson*, 1995]. It scales with plate thermal thickness T_{th}, excess mass of the slab with respect to the mantle $\Delta\rho$, gravity acceleration g, and slab's length L,

$$F_{sp} = 0.25\Delta\rho g T_{th} L \tag{1}$$

$$T_{th} = 2.32\sqrt{\kappa A}, \tag{2}$$

[27] [*Turcotte and Schubert*, 1982], κ being the thermal diffusivity, and A being the slab's age in seconds. The coefficient 0.25 accounts for the decreasing of the excess mass of the slab with depth [*Carlson et al.*, 1983]. F_{sp} exerts a bending torque M_{sp} at the pivot that contributes to the downward folding of the slab at the hinge. Except for buoyant subducting plates, this torque transmits an oceanward pressure along the interface between the plates. M_{sp} is the product of F_{sp} with the lever arm between the hinge and the gravity center of the slab (Figure 7),

$$M_{sp} = F_{sp}\frac{L}{2}\cos\alpha \tag{3}$$

Keeping L and α constant, the bending torque M_{sp} is proportional to the age of the subducting lithosphere at trench A since $\Delta\rho$ is a direct function of T_{th}.

[28] 2. Within the lithosphere, the main resisting force is related to the bending of the lithosphere at trenches. We use an elastic rheology for the slab as a proxy because of the lack of constraints to adjust an "efficient bending" viscosity for a viscous slab at trench. For a semifinite elastic slab, the bending moment M_b is the flexural rigidity of the plate D divided by its mean radius of curvature R_b [*Turcotte and Schubert*, 1982],

$$M_b = \frac{D}{R_b} \tag{4}$$

$$D = \frac{E(T_e)^3}{12(1-\nu^2)}, \tag{5}$$

where E and ν are the mean Young modulus and Poisson ratio, respectively, and

$$T_e = 4.2 \times 10^3\sqrt{A} \tag{6}$$

is the elastic thickness in meters with A (expressed in Ma) [see *McNutt*, 1984]. The torque M_b resists the bending of the lithosphere and thus exerts an arcward pressure along the

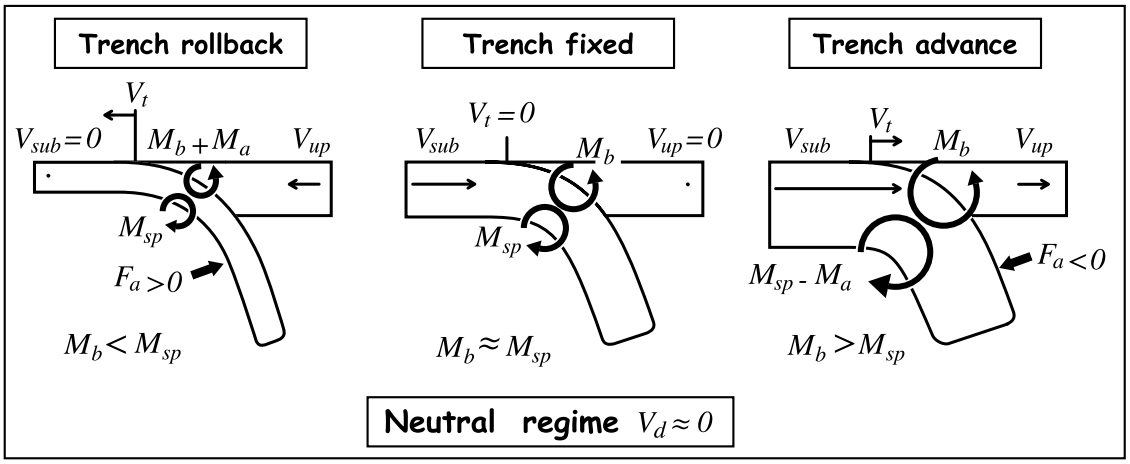

Figure 8. Sketch showing the balance of torques for the three examples illustrated in Figure 5. The slab pull torque M_{sp} increases with the age of the subducting plate A, as does V_{sub} if we consider that it is the main driving force for the subducting plate (see explanations in section 3.3). The mantle reaction to slab migration generates an anchoring torque M_a which tends to unbend the plate when the trench rolls back and to bend it when the trench is advancing.

interface between the plates. Assuming a constant R_b and a constant α, the moment M_b then increases with $A^{3/2}$.

[29] 3. There is an additional force F_a that accounts for the mantle reaction to slab facewise translation, including toroidal and poloidal flows. Some equations have been proposed by *Dvorkin et al.* [1993] or *Scholz and Campos* [1995] on the basis of the translation of an ellipsoid through a viscous fluid [*Lamb*, 1993]. In this study, we propose a simpler analytical solution adapted from work by *Panton* [1996] who considers the motion of an oblate spheroid (disk) into an infinite viscous fluid. The anchoring force F_a is thus estimated as

$$F_a = \frac{6\pi(3+2e)}{5} a\eta_m U_N, \tag{7}$$

and the viscous shear force F_{sh} is estimated as

$$F_{sh} = \frac{6\pi(4+e)}{5} a\eta_m U_T, \tag{8}$$

where $e < 1$ is the ratio between the disk radius a and its thickness taken as 1/4 if we consider a "circular" slab with L = 800 km and T_{th} = 100 km. Here η_m is the average viscosity of the displaced mantle, and U is the translation rate with normal and tangential components U_N and U_T with respect to the slab surface (see Figure 7),

$$U_N = V_t \sin\alpha \tag{9}$$

$$U_T = \nu_s + V_t \cos\alpha. \tag{10}$$

[30] The viscous drag acting on both sides of the descending slab does not produce any torque at the slab hinge. We will thus only consider the anchoring force in this balance. To be compared with the first two forces, F_a is normalized to the slab's width taken as equal to L, since we consider a "circular slab" in this equation. Here a should thus be replaced by a/L which is equal to 1/2. The simplified equation of the anchoring force thus becomes

$$F_a = 6.6\eta_m V_t \sin\alpha, \tag{11}$$

and the anchoring torque becomes

$$M_a = F_a \frac{L}{2}. \tag{12}$$

[31] For a given mantle viscosity η_m, dip angle α, and slab length L, this torque scales with the facewise translation rate $U_N = V_t \sin\alpha$. The force is directed either arcward or oceanward depending on the sense of slab motion, since it resists slab forward or backward motion.

[32] Assuming no stress transmission through the plates' interface (no significant deformation of the supposedly weak arc), we balance the oceanward/folding and arcward/unfolding torque components of these three forces (Figure 8), taking into account that in steady state, the sum of the moments should be zero. We write that

$$M_{sp} = M_b + M_a, \tag{13}$$

M_a being positive in the case of slab rollback, null for a fixed trench, and negative in the case of an advancing slab. These situations correspond to low, moderate, and high V_{sub}, respectively. The three examples in Figure 8 correspond to those illustrated in Figure 5.

[33] Let us consider three subduction systems (Figure 8) with the same length L = 700 km, dip $\alpha = 50°$, and radius of curvature of subducting slabs R_b = 350 km and values for

Table 3. Parameters Used in the Calculations and Notations[a]

Quantity	Symbol	Value (Range)
Thermal diffusivity	κ	10^{-6} m^2 s^{-1}
Gravity acceleration	g	9.81 m s^{-2}
Young modulus	E	155 GPa
Poisson ratio	ν	0.28
Asthenosphere viscosity	η_m	10^{19}–10^{21} Pa s
Crustal density	ρ_c	2900 kg m^{-3}
Lithospheric mantle density	ρ_{lm}	3300 kg m^{-3}
Asthenosphere density	ρ_a	3230 kg m^{-3}

[a]Young modulus and Poisson ratio are given for a range of subducting lithospheres aged 10 to 140 Ma [*Meissner*, 1986].

the other parameters as listed in Table 3. We compare in Table 4 the behavior of five cases, including the three ones mentioned in Figure 8, with various ages of subducting lithospheres, 20, 60, 80, 100 and 140 Ma and respective trench absolute velocities V_t, −2.5, 0, +2.5 and +5 cm a^{-1}. According to *Cloos* [1993], we can estimate the bulk density of an oceanic plate from those of a 7 km thick oceanic crust and a lithospheric mantle whose thickness is deduced from the total thermal thickness T_{th} (see equation (2)). This allows us to calculate the excess mass $\Delta\rho$ for each slab, taking mean densities for the crust, lithospheric mantle, and asthenosphere as given in Table 3.

[34] We observe in Table 4 that M_b is lower than M_{sp} for young slabs, except the very young ones for which M_{sp} can become negative, and exceeds M_{sp} for old ones. Using our values (see Table 3), the change happens for slabs aged about 80 Ma for which $M_b \cong M_{\text{sp}}$. Slab pull forces F_{sp} vary from 2.2 to 13.7 10^{12} N per unit length of trench, leading to a slab pull moment M_{sp} from 0.5 to 3.1 10^{18} N m in the range of slabs aged between 20 and 140 Ma at trench, whereas the bending moment M_b varies from 0.3 to 4.9 10^{18} N m. The anchoring force F_a both depends on slab facewise translation velocity $V_t\sin\alpha$ and mantle viscosity η_m. Table 4 is thus only indicative of tendencies but should be adapted depending on some key parameters like η_m, which is a matter of debate between low values, 10^{19} to 10^{20} Pa s, and higher ones, 10^{21} to 10^{22} Pa s [*Winder and Peacock*, 2001; *Cadek and Fleitout*, 2003; *Mitrovica and Forte*, 2004; *Enns et al.*, 2005]. If we use 10^{21} instead of 10^{20} Pa s, then our anchoring moments will increase by a factor of 10. All other parameters may also vary, like L, α, R_b, $\Delta\rho$, or the slab width. Ultimately, we have chosen to consider a passive mantle that opposes to slab facewise migration, but we have evidence of mantle flow in various regions, especially around slab lateral edges, as in Tonga. In this case, we must count with an additional force exerted by the mantle onto the slab.

[35] From the balance of forces and earlier observations, we can say that arcward trench motion (advancing) is marked by high resistance of the plate to bending at the trench together with a quickly subducting plate, and that the opposite occurs for trench rollback. This explains the negative correlation between the age of the lithosphere at trench A and V_t [*Heuret and Lallemand*, 2005], i.e., trench rollback for young subducting plates and vice versa together with the positive correlation between A and V_{sub} (Figure 3). Such observations highlight the role of the bending resistance that scales with the cube of the square root of A, whereas the slab pull scales with A only. It is therefore dominant for old (and fast) subducting plates [*Conrad and Hager*, 1999; *Becker et al.*, 1999; *Faccenna et al.*, 2007]. *Di Giuseppe et al.* [2008] also pointed out the competition between slab stiffness and slab pull. They concluded that advancing-style subduction is promoted by thick plate, a large viscosity ratio, or a small density contrast between plate and mantle. On the basis of 2-D numerical models with a viscosity structure constrained by laboratory experiments for the deformation of olivine, *Billen and Hirth* [2007] also concluded that the slab stiffness has a stronger affect on dynamics than small differences in slab density due to plate age.

[36] In our model, we have pointed out how the lithosphere and the mantle together control trench migration. We consider that the classification of transects into three groups (extensional, neutral, and compressional) as a function of V_{sub} and V_{up} is another positive argument in favor of the HS3 reference frame.

[37] One important point is that back arc rifting or spreading is not necessarily related to trench rollback, even in the SB04 reference frame (see Izu-Bonin, Kermadec, or Andaman). These behaviors are the result of a specific combination of V_{sub} and V_{up} that favors either extension or compression.

4. Conclusions

[38] By selecting modern subduction zones for which the overriding plates do not deform significantly, we have explored the kinematics of trenches with respect to both

Table 4. Estimates of Forces and Related Torques for Various Slab Ages and Trench Migration Rates[a]

	A (Ma)	Te (km)	T_{th} (km)	$\Delta\rho$ (kg m^{-3})	D (10^{22} N m)	v_t (cm a^{-1})	F_{sp} (10^{12} N)	F_a (10^{12} N)	M_{sp} (10^{18} N m)	M_a (10^{18} N m)	M_b (10^{18} N m)
Trench rollback	20	18.8	58.3	22.0	9.3	−2.5	2.20	2.00	0.50	0.14	0.26
Fixed trench	60	32.5	100.9	42.2	49.0	0	7.31	0	1.64	0	1.40
Advancing trench	80	37.6	116.5	46.0	74.5	2.5	9.20	−2.00	2.07	−0.14	2.13
Advancing trench	100	42.0	130.3	48.5	103.8	2.5	10.85	−2.00	2.44	−0.14	2.97
Advancing trench	140	49.7	154.2	51.8	172.0	5.0	13.70	−4.00	3.09	−0.28	4.91

[a]See section 2 for the definition of parameters and Table 3 for the values used in the calculations. We have used $\eta_m = 10^{20}$ Pa s. Analogies can be found with modern subduction zones such as Cascades (A = 10 Ma, rollback, V_t = −2.5 cm a^{-1}, α = 45°), Luzon (A = 20 Ma, rollback, V_t = −8 cm a^{-1}, α = 70°), eastern Aleutian (A = 60 Ma, advance, V_t = 0.5 cm a^{-1}, α = 60°), Java (A = 80 Ma, advance, V_t = 1.5 cm a^{-1}, α = 70°), Kamtchatka (A = 100 Ma, advance, V_t = 2 cm a^{-1}, α = 60°), northern Kuril (A = 110 Ma, advance, V_t = 2 cm a^{-1}, α = 50°), and Izu-Bonin (A = 140 Ma, advance, V_t = 5 cm a^{-1}, α = 70°).

the behaviors of the subducting plate (rheology and kinematics) and the reaction of the mantle. We have shown that neutral subduction zones satisfy a combination of velocities: $V_{sub} - 2V_{up} = 4.6$ cm a^{-1} in the HS3 reference frame. For higher V_{sub}, trenches advance faster than the upper plates retreat, and compression is favored, whereas for lower V_{sub}, trenches retreat faster than the upper plates advance, favoring extension. In the neutral domain, in which $V_t = V_{up}$, we have shown that spontaneous trench motion can occur either oceanward (rollback) for slow (and young) subducting plates or arcward (advance) for fast (and old) subducting plates. We implicitly treat the paradox of trench rollback that generally occurs with young slabs but not with old ones. We propose that this behavior is mainly caused by the resistance of the subducting plate to bending, as its stiffness (as well as its velocity) increases with age faster than the slab pull for plates older than 80 Ma.

[39] **Acknowledgments.** This research was supported by the CNRS-INSU DyETI program "Dynamics of Subduction" and as part of the Eurohorcs/ESF-European Young Investigators Awards Scheme, by funds from the National Research Council of Italy and other national funding agencies participating in the Third Memorandum of Understanding, as well as from the EC Sixth Framework Programme. We thank all our colleagues who participated in this program for the numerous discussions and debates and especially Neil Ribe and Jean Chéry. We also thank Richard Carlson and Wouter Schellart for their improvement of an earlier version of this paper, Thorsten Nagel and an anonymous reviewer for their constructive review, and Anne Delplanque for her precious help in line drawings.

References

Becker, T. W. (2006), On the effect of temperature and strain-rate dependent viscosity on global mantle flow, net rotation, and plate-driving forces, *Geophys. J. Int.*, *167*, 943–957, doi:10.1111/j.1365-246X.2006.03172.x.

Becker, T. W., C. Faccenna, R. J. O'Connell, and D. Giardini (1999), The development of slabs in the upper mantle: Insights from numerical and laboratory experiments, *J. Geophys. Res.*, *104*(B7), 15,207–15,226, doi:10.1029/1999JB900140.

Bellahsen, N., C. Faccenna, and F. Funiciello (2005), Dynamics of subduction and plate motion in laboratory experiments: Insights into the "plate tectonics" behavior of the Earth, *J. Geophys. Res.*, *110*, B01401, doi:10.1029/2004JB002999.

Billen, M. I., and G. Hirth (2007), Rheologic controls on slab dynamics, *Geochem. Geophys. Geosyst.*, *8*, Q08012, doi:10.1029/2007GC001597.

Buffett, B. A., and D. B. Rowley (2006), Plate bending at subduction zones: Consequences for the direction of plate motions, *Earth Planet. Sci. Lett.*, *245*, 359–364, doi:10.1016/j.epsl.2006.03.011.

Cadek, O., and L. Fleitout (2003), Effect of lateral viscosity variations in the top 300 km on the geoid and dynamic topography, *Geophys. J. Int.*, *152*, 566–580, doi:10.1046/j.1365-246X.2003.01859.x.

Carlson, R. L. (1995), A plate cooling model relating rates of plate motion to the age of the lithosphere at trenches, *Geophys. Res. Lett.*, *22*(15), 1977–1980, doi:10.1029/95GL01807.

Carlson, R. L., and P. J. Melia (1984), Subduction hinge migration, *Tectonophysics*, *102*, 399–411.

Carlson, R. L., T. W. C. Hilde, and S. Uyeda (1983), The driving mechanism of plate tectonics: Relation to age of the lithosphere at trench, *Geophys. Res. Lett.*, *10*(4), 297–300.

Chase, C. G. (1978), Plate kinematics: The Americas, East Africa, and the rest of the world, *Earth Planet. Sci. Lett.*, *37*, 355–368, doi:10.1016/0012-821X(78)90051-1.

Cloos, M. (1993), Lithospheric buoyancy and collisional orogenesis: Subduction of oceanic plateaus, continental margins, island arcs, spreading ridges and seamounts, *Geol. Soc. Am. Bull.*, *105*(6), 715–737, doi:10.1130/0016-7606(1993)105<0715:LBACOS>2.3.CO;2.

Conrad, C. P., and B. H. Hager (1999), Effects of plate bending and fault strength at subduction zones on plate dynamics, *J. Geophys. Res.*, *104*(B8), 17,551–17,571, doi:10.1029/1999JB900149.

Conrad, C. P., and C. Lithgow-Bertelloni (2002), How mantle slabs drive plate tectonics, *Science*, *298*, 207–209, doi:10.1126/science.1074161.

Currie, C. A., and R. D. Hyndman (2006), The thermal structure of subduction zone back arcs, *J. Geophys. Res.*, *111*, B08404, doi:10.1029/2005JB004024.

Davies, G. F. (1980), Mechanics of subducted lithosphere, *J. Geophys. Res.*, *85*(B11), 6304–6318, doi:10.1029/JB085iB11p06304.

DeMets, C., R. G. Gordon, D. F. Argus, and S. Stein (1994), Effect of recent revisions to the geomagnetic reversal time scale on estimates of current plate motion, *Geophys. Res. Lett.*, *21*(20), 2191–2194.

Dewey, J. F. (1980), Episodicity, sequence and style at convergent plate boundaries, in *The Continental Crust and Its Mineral Deposits*, edited by D. W. Strangway, *Spec. Pap. 20*, pp. 553–573, Geol. Assoc. of Can., St. John's, Nfld., Canada.

Di Giuseppe, E., J. van Hunen, F. Funiciello, C. Faccenna, and D. Giardini (2008), Slab stiffness control of trench motion: Insights from numerical models, *Geochem. Geophys. Geosyst.*, *9*, Q02014, doi:10.1029/2007GC001776.

Doglioni, C., E. Carminati, M. Cuffaro, and D. Scrocca (2007), Subduction kinematics and dynamic constraints, *Earth Sci. Rev.*, *83*(3–4), 125–175, doi:10.1016/j.earscirev.2007.04.001.

Dvorkin, J., A. Nur, G. Mavko, and Z. Ben-Avraham (1993), Narrow subducting slabs and the origin of back-arc basins, *Tectonophysics*, *227*, 63–79, doi:10.1016/0040-1951(93)90087-Z.

Enns, A., T. W. Becker, and H. Schmelling (2005), The dynamics of subduction and trench migration for viscosity stratification, *Geophys. J. Int.*, *160*, 761–775, doi:10.1111/j.1365-246X.2005.02519.x.

Faccenna, C., A. Heuret, F. Funiciello, S. Lallemand, and T. Becker (2007), Predicting trench and plate motion from the dynamics of a strong slab, *Earth Planet. Sci. Lett.*, *257*, 29–36, doi:10.1016/j.epsl.2007.02.016.

Forsyth, D. W., and S. Uyeda (1975), On the relative importance of the driving forces of plate motion, *Geophys. J.R. Astron. Soc.*, *43*, 163–200.

Funiciello, F., C. Faccenna, and D. Giardini (2004), Role of lateral mantle flow in the evolution of subduction systems: Insights from laboratory experiments, *Geophys. J. Int.*, *157*, 1393–1406, doi:10.1111/j.1365-246X.2004.02313.x.

Funiciello, F., C. Faccenna, A. Heuret, S. Lallemand, E. Di Giuseppe, and T. W. Becker (2008), Trench migration, net rotation and slab-mantle coupling, *Earth Planet. Sci. Lett.*, doi:10.1016/j.epsl.2008.04.006, in press.

Garfunkel, Z., C. A. Anderson, and G. Schubert (1986), Mantle circulation and the lateral migration of subducted slabs, *J. Geophys. Res.*, *91*(B7), 7205–7223, doi:10.1029/JB091iB07p07205.

Gripp, A. E., and R. G. Gordon (2002), Young tracks of hotspots and current plate velocities, *Geophys. J. Int.*, *150*, 321–361, doi:10.1046/j.1365-246X.2002.01627.x.

Hamilton, W. B. (2003), An alternative Earth, *GSA Today*, *13*, 4–12, doi:10.1130/1052-5173(2003)013<0004:AAE>2.0.CO;2.

Heuret, A. (2005), Dynamique des zones de subduction: Etude statistique globale et approche analogique, Ph.D. thesis, 235 pp., Montpellier II Univ., Montpellier, France, 16 Nov.

Heuret, A., and S. Lallemand (2005), Plate motions, slab dynamics and back-arc deformation, *Phys. Earth Planet. Inter.*, *149*, 31–51, doi:10.1016/j.pepi.2004.08.022.

Heuret, A., F. Funiciello, C. Faccenna, and S. Lallemand (2007), Plate kinematics, slab shape and back-arc stress: A comparison between laboratory models and current subduction zones, *Earth Planet. Sci. Lett.*, *256*, 473–483, doi:10.1016/j.epsl.2007.02.004.

Jarrard, R. D. (1986), Relations among subduction parameters, *Rev. Geophys.*, *24*(2), 217–284, doi:10.1029/RG024i002p00217.

Lagabrielle, Y., J. Goslin, H. Martin, J.-L. Thirot, and J.-M. Auzende (1997), Multiple active spreading centres in the hot North Fiji Basin (Southwest Pacific): A possible model for Archean seafloor dynamics?, *Earth Planet. Sci. Lett.*, *149*, 1–13, doi:10.1016/S0012-821X(97)00060-5.

Lallemand, S., A. Heuret, and D. Boutelier (2005), On the relationships between slab dip, back-arc stress, upper plate absolute motion, and crustal nature in subduction zones, *Geochem. Geophys. Geosyst.*, *6*, Q09006, doi:10.1029/2005GC000917.

Lamb, C. (1993), *Hydrodynamics*, 6th ed., 738 pp., Cambridge Univ. Press, New York.

McKenzie, D. P. (1977), The initiation of trenches: A finite amplitude instability, in *Island Arcs, Deep-Sea Trenches, and Back-Arc Basins, Maurice Ewing Ser.*, vol. 1, edited by M. Talwani and W. C. Pitman, pp. 57–61, AGU, Washington, D. C.

McNutt, M. K. (1984), Lithospheric flexure and thermal anomalies, *J. Geophys. Res.*, *89*(B13), 11,180–11,194, doi:10.1029/JB089iB13p11180.

Meissner, R. (1986), *The Continental Crust: A Geophysical Approach,* vol. 34, 426 pp., Elsevier, London.

Mitrovica, J. X., and A. M. Forte (2004), A new inference of mantle viscosity based upon joint inversion of convection and glacial isostatic adjustment data, *Earth Planet. Sci. Lett.*, *225*, 177–189, doi:10.1016/j.epsl.2004.06.005.

Molnar, P., and T. Atwater (1978), Interarc spreading and cordilleran tectonics as alternates related to the age of subducted oceanic lithosphere, *Earth Planet. Sci. Lett.*, *41*, 827–857, doi:10.1016/0012-821X(78)90187-5.

Otsuki, K. (1989), Empirical relationships among the convergence rate of plates, rollback rate of trench axis and island-arc tectonics: Laws of convergence rate of plates, *Tectonophysics*, *159*, 73–94, doi:10.1016/0040-1951(89)90171-6.

Pacanovsky, K. M., D. M. Davis, R. M. Richardson, and D. D. Coblentz (1999), Intraplate stresses and plate-driving forces in the Philippine Sea plate, *J. Geophys.*

Res., *104*(B1), 1095–1110, doi:10.1029/98JB02845.

Panton, R. L. (1996), *Incompressible Flow*, 2nd ed., 910 pp., John Wiley, New York.

Pelletier, B., S. Calmant, and R. Pillet (1998), Current tectonics of the Tonga-New Hebrides region, *Earth Planet. Sci. Lett.*, *164*, 263–276, doi:10.1016/S0012-821X(98)00212-X.

Schellart, W. P. (2005), Influence of the subducting plate velocity on the geometry of the slab and migration of the subduction hinge, *Earth Planet. Sci. Lett.*, *231*, 197–219, doi:10.1016/j.epsl.2004.12.019.

Scholz, C. H., and J. Campos (1995), On the mechanism of seismic decoupling and back-arc spreading at subduction zones, *J. Geophys. Res.*, *100*(B11), 22,103–22,115, doi:10.1029/95JB01869.

Steinberger, B., R. Sutherland, and R. J. O'Connell (2004), Prediction of Emperor-Hawaii seamount locations from a revised model of global motion and mantle flow, *Nature*, *430*, 167–173, doi:10.1038/nature02660.

Turcotte, D. L., and G. Schubert (1982), *Geodynamics: Applications of Continuum Physics to Geological Problems*, 450 pp., John Wiley, New York.

Winder, R. O., and S. M. Peacock (2001), Viscous forces acting on subducting lithosphere, *J. Geophys. Res.*, *106*(B10), 21,937–21,951, doi:10.1029/2000JB000022.

C. Faccenna and F. Funiciello, Dipartimento di Scienze Geologiche, Università degli Studi Roma TRE, I-00146 Roma, Italy.

A. Heuret and S. Lallemand, UMR 5573, CNRS, Laboratoire Géosciences Montpellier, Montpellier II Université, Case 60 Place E. Bataillon, F-34095 Montpellier Cédex 05, France. (lallem@gm.univ-montp2.fr)